Annales Societatis Geologorum Poloniae (2025), vol. 95: 45–61 https://doi.org/10.14241/asgp.2025.05

STRUCTURAL AND THERMOCHRONOLOGIC INVESTIGATION ACROSS THE WESTERN POLISH OUTER CARPATHIANS: A RECONNAISSANCE STUDY

Jan BARMUTA[1]*, **Saeideh Asal SEYEDI**[2], **Lothar RATSCHBACHER**[2] **& Krzysztof STARZEC**[3]

[1] *Institute of Geological Sciences, Polish Academy of Sciences, Senacka 1, 31-002 Kraków, Poland; e-mail: ndbarmut@cyf-kr.edu.pl*

[2] *Institut für Keramik, Feuerfest und Verbundwerkstoffe, Technische Universität Bergakademie, Agricolastraße 17, 09599 Freiberg, Germany; e-mails: saeideh.seyedi@doktorand.tu-freiberg.de, Lothar.Ratschbacher@extern.tu–freiberg.de*

[3] *AGH University of Krakow, Faculty of Geology, Geophysics and Environmental Protection, Mickiewicza 30, 30-059 Kraków, Poland; e-mail: kstarzec@agh.edu.pl*

** Corresponding author*

Barmuta, J., Seyedi, A. S., Ratschbacher, L. & Starzec, K., 2025. Structural and thermochronologic investigation across the Western Polish Outer Carpathians: a reconnaissance study. *Annales Societatis Geologorum Poloniae*, 95: 45–61.

Abstract: A regional cross-section based on geophysical, borehole, and structural field data reveals the subsurface structure of the western Polish Outer Carpathians, a relatively understudied segment of the Carpathian thrust-and-fold belt. A key feature is an antiformal stack, where the Dukla Unit underlies the central part of the Magura Unit. This structure probably was formed due to a thrust ramp within the Palaeozoic cover of the North European Platform. New apatite fission-track ages, along with a re-evaluation of published thermochronologic age data, indicate two exhumation phases. The first occurred in the Early Miocene (~20 Ma), affecting the Magura and Silesian units. The second, in the Late Miocene (~10 Ma), is confined to the Magura Unit and linked to an antiformal stack formation either through underthrusting of the Magura Unit by the Dukla Unit or large-scale normal faulting that drove arc-parallel extension. Both structures are supported by outcrop and seismic evidence. The present authors propose that the lateral termination of the antiformal stack triggered a normal fault system, forming a hanging-wall drop fault along a lateral culmination wall. The structural data of the present study do not support a Middle–Late Miocene arc-perpendicular extension, previously documented in the eastern Polish Outer Carpathians, as a viable explanation for the Late Miocene exhumation, recorded in the western sector.

Key words: Outer Carpathians, apatite fission track, tectonic evolution, arc-parallel extension, seismic interpretation.

Manuscript received 7 September 2024, accepted 30 May 2025

INTRODUCTION

Understanding the evolution of fold-and-thrust belts requires the integration of various analytical methods, including geophysical investigations, structural analysis, cross-section balancing, structural forward modelling, and thermochronologic dating to reconstruct the temperature-time paths to facilitate the interpretation of their burial and exhumation histories (e.g., Brückl *et al.*, 2010; Nakapelyukh *et al.*, 2018; Buford Parks and McQuarrie, 2019; Abdulhameed *et al.*, 2020; Gągała *et al.*, 2020; Roger *et al.*, 2023).

The Outer Carpathians fold-and-thrust belt (OC) is a Cenozoic accretionary wedge that was formed through the accretion of multiple basins along the extended passive margin of the North European Platform (NEP; Fig. 1; e.g., Książkiewicz, 1958, 1977; Morley, 1996; Nemčok *et al*., 2001; Oszczypko *et al*., 2003; Golonka *et al*., 2006; Cieszkowski *et al*., 2009; Kováč *et al*., 2016, 2017; Schmid *et al*., 2020). In the Polish Outer Carpathians (POC), numerous studies have used structural restorations and thermochronologic dating to determine the style, magnitude, and timing of shortening and exhumation (Roure *et al*., 1993; Roca *et al*., 1995; Roure and Sassi, 1995; Nemčok *et al*., 2006a, b; Mazzoli *et al*., 2010; Zattin *et al*., 2011; Gągała *et al*., 2012; Andreucci *et al*., 2013; Castelluccio *et al*., 2015, 2016). Most of these studies focused on the central and eastern POC and typically employed either structural reconstruction or

thermochronologic dating. Their findings revealed significant differences between the central and eastern POC compared to the western POC: (1) shortening increases eastward, despite variations in reconstruction methodologies and datasets (e.g., Castelluccio *et al*., 2016), and (2) apatite fission-track (AFT) ages show an eastward-younging trend (Mazzoli *et al*., 2010; Zattin *et al*., 2011), reflecting the progressive eastward development of the fold-and-thrust belt.

The terminal thrusting along the leading edge of the belt is estimated to have occurred between 17–15 Ma in the Czech-Polish OC (Jiřiček, 1979; Nemčok *et al*., 1998a, 2006a), around 12 Ma in the Ukrainian OC (Nakapelyukh *et al*., 2018; Roger *et al*., 2023), and approximately 10 Ma in the Romanian OC (e.g., Matenco and Bertotti, 2000).

To investigate the tectonic evolution of the western POC, the present authors constructed a regional cross-section extending from the Pieniny Klippen Belt to the OC foredeep (Fig. 1). They collected and analysed structural field data from key outcrops and conducted apatite fission-track (AFT) analysis on 10 samples along the section line. This reconnaissance effort represents an initial step toward addressing a gap in the thermochronologic database for the POC, aiming to integrate the results with structural observations from outcrops and geophysical subsurface interpretations (Barmuta *et al*., 2021; Mikołajczak *et al*., 2021). The present authors also compared their AFT and structural data with those of existing literature, highlighting both similarities and differences in the tectonic evolution of the eastern and western POC.

GEOLOGICAL SETTING

The OC fold-and-thrust belt is a part of the thin-skinned Carpathian arc that stretches from Austria to Romania. It is composed of thrust sheets, widely referred to as 'nappes' or 'units'. In Poland, the following units can be distinguished from south to north: the Magura Unit, a group of Fore-Magura Units, comprising the Dukla, Grybów, and Obidowa-Słopnice units, and the Silesian, Subsilesian, and Skole units (Fig. 1). These units were thrust onto the NEP during the Oligocene–Miocene (ca. 33 to 8 Ma; Jiřiček, 1979; Wójcik and Jugowiec, 1998; Wójcik *et al.,* 2001; Zuchiewicz *et al.,* 2001; Sperner *et al.,* 2002; Golonka *et al.,* 2006; Nemčok *et al.,* 2006a; Beidinger and Decker, 2016). On the basis of lithostratigraphic differences (Fig. 2), each unit is interpreted as the sedimentary sequence of a separate basin (or a part of it), which was detached and thrust onto its foreland (e.g., Ślączka *et al.,* 2006).

The Magura Unit with its second order thrust sheets – the Krynica, Bystrica, Rača, and Siary subunits – occupies the southern part of the western POC (Fig. 1; e.g., Oszczypko and Oszczypko-Clowes, 2009). The oldest rocks of the Magura Unit belong to the Upper Cretaceous Malinowa Shale Formation, followed by the Ropianka Formation and its stratigraphic equivalent, the Jaworzynka Formation (Teťák *et al.,* 2017; Fig. 2). Higher in the stratigraphic sequence, a thin horizon of deep-water variegated shales, the Eocene Łabowa Shale Formation, marks the onset of deposition of a thick turbidite fan system represented by the Eocene–Oligocene Magura Formation of the Bystrica and Rača subunits and the Oligocene Zembrzyce Beds of the Siary Subunit. These formations were deposited during the main phase of thrusting within the Magura Basin (Oszczypko and Oszczypko-Clowes, 2009). The front of the Magura Unit is occupied by the narrow Dukla Unit, comprising Upper Cretaceous to Oligocene formations (Burtan *et al.*, 1973; Paul *et al.*, 1996; Starzec *et al.,* 2014; Ryłko, 2018). Interpretation of seismic data allowed the tracing of this unit below the basal thrust of the Magura Unit (Barmuta *et al.,* 2019, 2021). Further north, the broad Silesian Unit comprises a ca. 6 km thick Upper Jurassic–Oligocene sedimentary sequence, with the Upper Cretaceous–lowermost Paleocene Godula and Istebna Beds covering c. 4 km (Słomka and Słomka, 2001; Strzeboński, 2015, 2022). Structurally, the Silesian Unit is divided into the southern Godula and northern Cieszyn subunits; the former constitutes a south-dipping homocline, probably including the entire sedimentary sequence of the Silesian Unit, while the latter comprises only Upper Jurassic–Lower Cretaceous rocks stacked into closely-spaced thrust slices.

The northernmost Subsilesian Unit, interpreted as an equivalent of the Ždánice Unit in the Czech Republic (Stráník, 1963; Elias, 1992; Picha and Stráník, 1999; Lexa *et al.,* 2000; Picha *et al.,* 2006), crops out in a narrow zone in front of the Silesian Unit and in tectonic windows (Fig. 1). For simplification, the present authors incorporated the intensively deformed Miocene Andrychów Series (Wójcik and Jugowiec, 1998; Wójcik *et al.,* 2001; Połtowicz, 2004) into the Subsilesian Unit.

OVERVIEW OF STRUCTURAL AND THERMOCHRONOLOGIC STUDIES

Early computer-aided attempts to quantify shortening in the POC fold-and-thrust belt suggested at least 180 km for the central sector (Bochnia-Zakopane line; Roca *et al.,* 1995) and at least 260 km for the eastern POC (the Przemyśl area; Roure *et al.,* 1993; Behrmann *et al.,* 2000). These authors also addressed fault reactivation in the basement of the NEP and the involvement of its Mesozoic cover in the fold-and-thrust belt. Nemčok *et al.,* (2001, 2006b) presented structural restorations along five cross-sections, spaced along the POC arc. For the westernmost cross-section, they estimated 58% (75 km) of shortening, resulting in 130 km of pre-deformed width of the Silesian Unit. For the Magura Unit, 32% (20 km) of shortening was obtained, which corresponds to 64 km of pre-deformed width of the basin These values represent the internal deformation of the units and not shortening of the entire fold-and-thrust belt. Gągała *et al.,* (2012) obtained higher shortening values, i.e., ca. 507 km for the eastern POC, from which ca. 130 km were assigned to the Silesian and Skole units. For the adjacent Ukrainian sector of the OC, Nakapelyukh *et al*., (2018) obtained 340–390 km of total shortening.

Studies combining thermochronologic, cross-section balancing, structural forward-modelling, and field structural investigations were led by Italian researchers in both the central and eastern POC (Mazzoli *et al.,* 2010; Zattin *et*

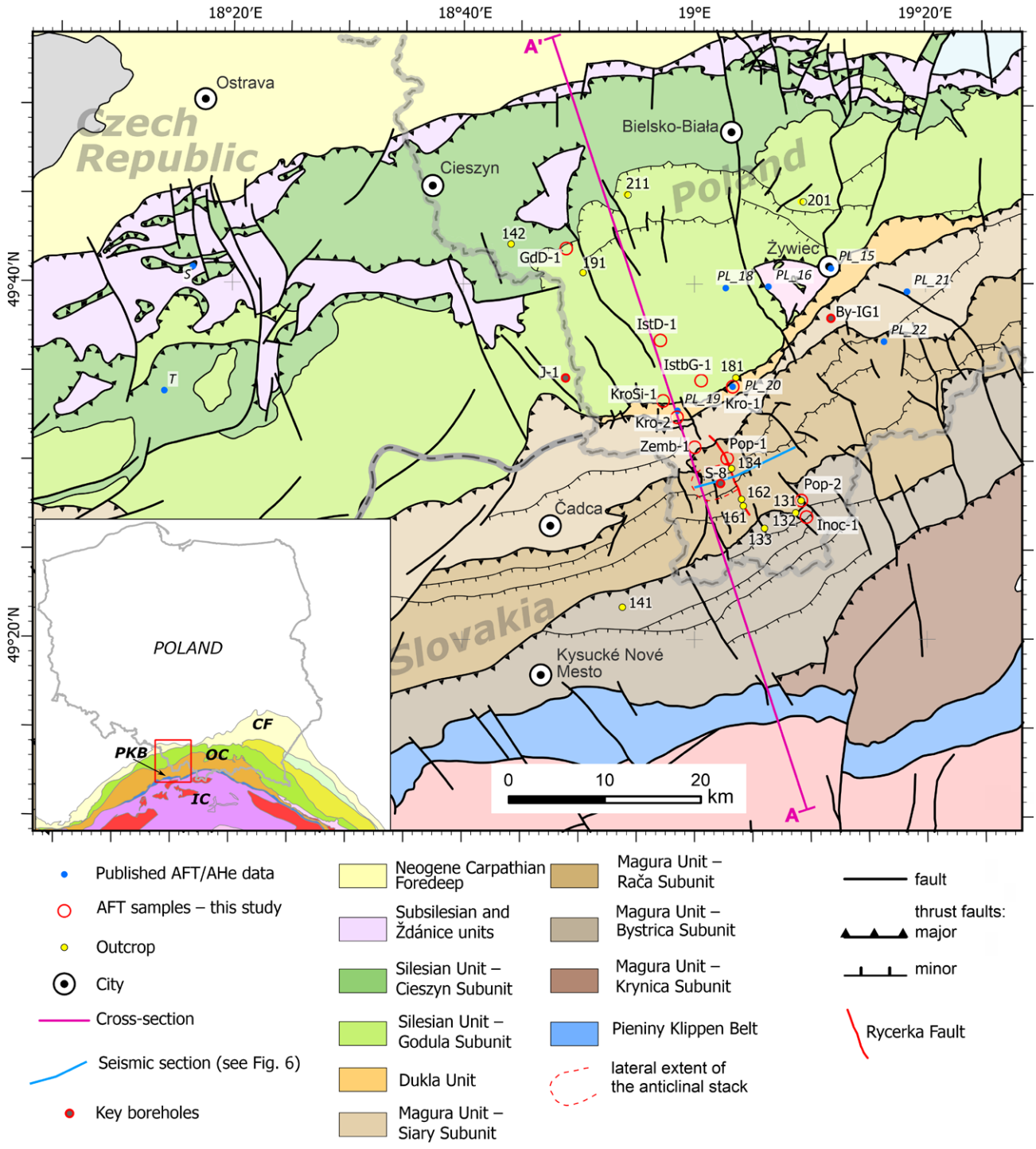

Fig. 1. Geological map of the western Polish Outer Carpathians fold-and-thrust belt with location of samples and exposures where structural analysis was performed. Lines of the cross-section (Fig. 3) and seismic profile (Fig. 6) are shown. Modified after Lexa *et al.* (2000) and Starzec *et al.* (2014). Boreholes: J-1 – Jablunkov-1, S-8 – Sól-8, By-IG1 – Bystra-IG1. Abbreviations in the inset: CF – Carpathian Foredeep, OC – Outer Carpathians, IC – Inner Carpathians, PKB – Pieniny Klippen Belt.

al., 2011; Andreucci *et al.,* 2013, 2014; Castelluccio *et al.,* 2015, 2016). For three regional cross-sections, they estimated, from west to east, ca. 135, 270, and 343 km for the initial width of the OC basins. Using low-temperature thermochronology, they estimated the volume of eroded rocks, improving the accuracy of the structural restorations. On the basis of the thermochronologic and structural studies, they documented two exhumation stages for the eastern POC fold-and-thrust belt and related them to: (i) stacking of units and associated erosion, lasting until ca. 11 Ma, and (ii) to post-orogenic, arc-perpendicular extension (ca. NNW–SSE) induced by normal faulting. According to these investigations, the post-orogenic exhumation affected the inner (southern) units of the central and eastern POC but was not recorded in the western POC belt. In contrast, comparably young AFT (<10 Ma, Late Miocene) ages from equivalent

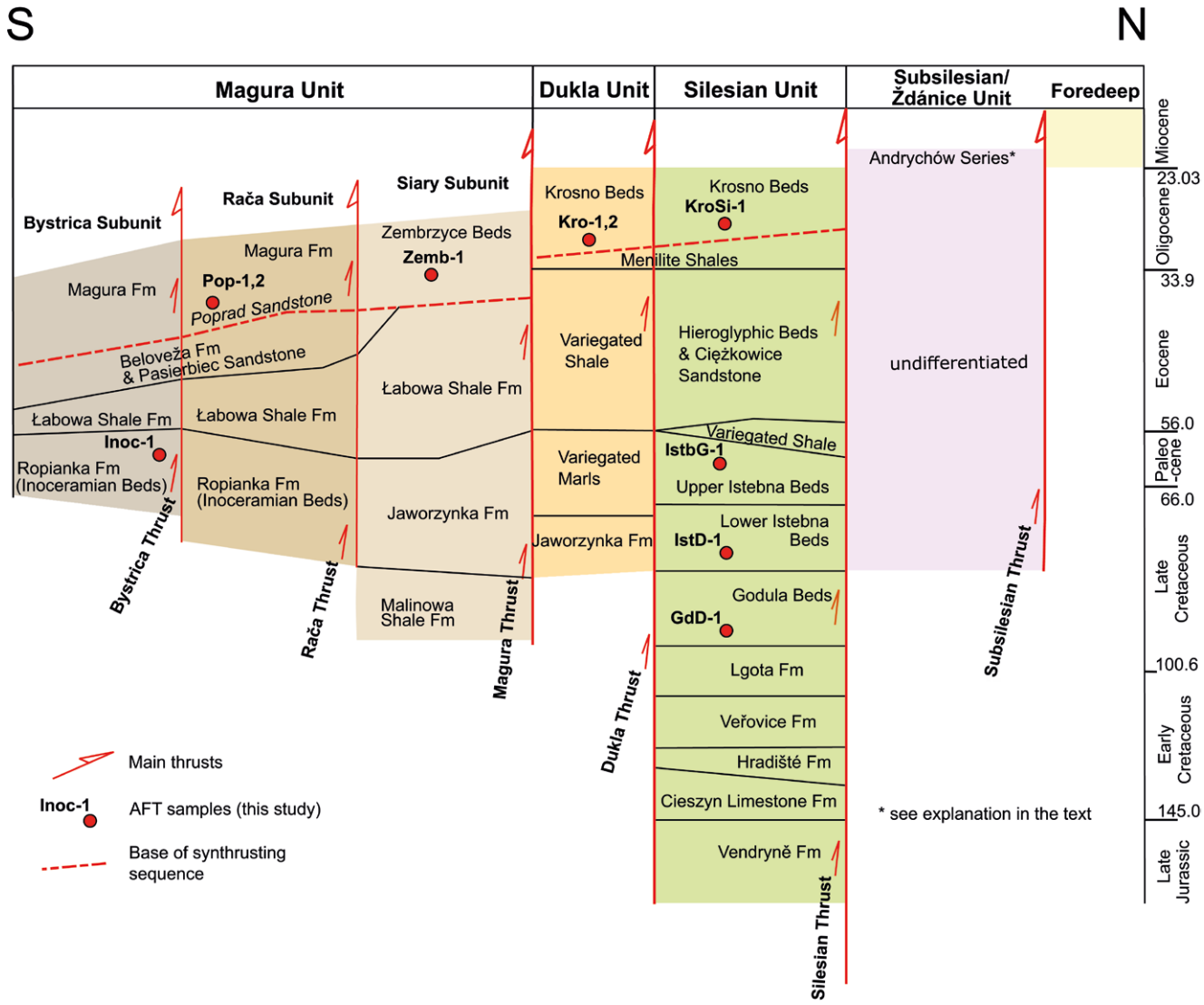

Fig. 2. Stratigraphic chart of the western Polish Outer Carpathians fold-and-thrust belt with the position of apatite fission-track samples from this study. Numerical values from International Stratigraphic Chart ICS 2023/04 (Cohen *et al.,* 2013). The stratigraphic scheme was compiled after Burtan *et al.* (1973), Nescieruk and Wójcik (2001), Oszczypko *et al.* (2005), Cieszkowski *et al.* (2007), Oszczypko and Oszczypko-Clowes (2009), Golonka and Waśkowska, (2012), Starzec *et al.* (2014), and Teťák *et al.* (2017).

units in the adjacent Ukrainian OC (Nakapelyukh *et al.,* 2018; Roger *et al.,* 2023) were interpreted as an effect of post-thrusting erosion of the thickened accretionary wedge, probably amplified by late out-of-sequence thrusting.

AFT combined with illite-smectite thermometric studies suggested two exhumation stages for the Magura Unit of the central POC (Świerczewska, 2005; Anczkiewicz and Świerczewska, 2008). The first was related to the formation and emplacement of the OC units onto the foreland (i.e., NEP) during the Eocene, while the second was associated with stacking within the Magura Unit and duplexing of the concealed Fore-Magura units, i.e., the Dukla, Obidowa-Słopnice, and Grybów units, below the Magura basal thrust. This caused exhumation in the hanging wall of the Magura Unit and the formation of tectonic windows. Temperature-time paths, obtained from AFT and apatite (U-Th)/He (AHe) data on two samples from the Cretaceous teschenites (a mafic sill intrusion) of the western Silesian Unit (samples T and S in Figure 1) indicated a late Eocene–early Oligocene onset of the accretion-related exhumation, and a main thrusting phase at ca. 20 Ma (Danišík *et al.,* 2008); the latter is in approximate agreement with the 17–15 Ma age for cessation of frontal thrusting in the western POC fold-and-thrust belt (Jiříček, 1979; Nemčok *et al.,* 2006a).

DATA AND METHODS

Cross-section construction

The authors constructed a regional cross-section interpreting the depth structure of the western POC fold-and-thrust belt and its substratum, on the basis of geophysical (Barmuta *et al.,* 2019, 2021; Mikołajczak *et al*., 2021) and geologic data (Fig. 3; Ryłko *et al.,* 1993; Potfaj *et al.,* 2002; Picha *et al.,* 2006; Plašienka *et al.,* 2021). The geophysical data included a seismic line crossing the Magura Unit as well as gravity and magnetic data that constrain the structure of the deep part of the fold-and-thrust belt and the

(semi)-autochthonous cover of the NEP. The shallow structure is based on surface geology provided by maps (Żytko, 1963; Burtan *et al.,* 1978; Nescieruk and Wójcik, 2001; Starzec *et al.,* 2014), dip measurements, and borehole logs, for which the basic information, such as stratigraphic profiles, were derived from the Central Geological Database (Central Geological Database 2024) managed by the Polish Geological Institute (http://baza.pgi.gov.pl/). Figure 3 also shows the new and published AFT and AHe ages, projected onto the cross-section plane. The projection was performed manually to locate the samples at the correct structural positions on the cross-section, following the strike of map-scale features, like folds and thrusts.

Apatite fission-track analysis

Apatite concentrates were produced by standard procedures, including crushing, sieving, magnetic and heavy-liquid separation, and handpicking. The dated grain-size range is 80–250 μm. As the apatites are from clastic rocks, their shapes are typical for detrital grains, anhedral, often rounded and fragmented. The authors determined the AFT ages with the external detector method (Gleadow, 1981; Hurford and Green, 1982). All mounts were etched for 20 s in 5.5 M HNO_3 at 21 °C (Carlson *et al.,* 1999), covered with muscovite external detectors, stacked in irradiation containers together with age-standard mounts (Durango apatite, 31.4 ± 0.5 Ma; Hurford, 1990; McDowell *et al.,* 2005), standard uranium glasses (IRMM–540R–A; Roebben *et al.,* 2006), and thermal and epithermal neutron-fluence monitors (Al–1% Co, IRMM–528R–A; Al–0.1% Co, IRMM–527R–A; Al–0.1% Au, IRMM–530R–A). All the dosimeters are 12–mm-diameter circular foils of 0.1 mm thickness. The samples were irradiated with a nominal neutron fluence of 5.0×10^{15} cm^{-2} in channel Y4 of the BR1 reactor (Mol, Belgium). The external detectors were etched for 30 min. in 48% HF at room temperature and repositioned track-side down on the apatite mounts for track counting (Jonckheere *et al*., 2003). Where prism faces could be identified, the authors measured Dpar, the maximum diameter of the fission-track etch figure parallel to the grain *c*-axis, as kinetic parameter (Burtner *et al.,* 1994). Table 1 summarizes the AFT data. Figure 4 compiles Abanico plots (Dietze *et al.,* 2016) for all samples; the Radial plots (Galbraith, 1988, 1990) include the stratigraphic age for each sample and were constructed using RadialPlotter (Vermeesch, 2009). The authors also used RadialPlotter to test for heterogeneous grain-age distributions (probability $P(\chi^2) \geq 0.05$ indicates a homogeneous distribution), calculated the dispersion, and, when appropriate, applied the mixture-modelling algorithm to derive age peaks in the distribution. For some samples, the authors calculated the mean and the standard deviation of grain ages that encompass the youngest reset grains in the age distribution (Fig. 4; Tab. 1). The authors define ages as reset, when they are younger than the stratigraphic age of the sample.

Structural analysis and seismic data

The fieldwork of the present study aimed at documenting structures (folds, faults, tension gashes, etc.) and their relative time evolution on an outcrop scale and to establish the kinematics of fault arrays. In particular, the authors aimed to find evidence for post-thrusting, arc-perpendicular extension in the western POC fold-and-thrust belt, as this event was interpreted as being responsible for young (<11 Ma) AFT ages in the eastern POC fold-and-thrust belt (Mazzoli *et al.,* 2010; Zattin *et al.,* 2011). For this purpose, the authors established the location, geometry, and kinematics of the brittle deformation features, grouping structures into 'sites-defined as single or closely-spaced outcrops with a consistent set of structural data. The observations were carried out in active and abandoned quarries and along rivers and are sparse, due to the outcrop conditions in the POC fold-and-thrust belt. To understand the kinematics of fault arrays, the authors applied stress-inversion techniques to fault-striae data, employing the 'numeric dynamic analysis' of Spang (1972), implemented by Sperner *et al.* (1993) and Sperner and Ratschbacher (1994), using the TectonicsFP software. Angelier (1984), Passchier and Trouw (2005), and Sperner and Zweigel (2010) gave summaries and assessments of these methods. As the main task of this part of the study was to identify potential post-thrusting extension within the inner nappes of the western POC fold-and-thrust belt, the authors only report data from outcrops located in the Magura Unit (Figs 1, 5; Tab. 2), where the assumed arc-perpendicular extension could be present. To establish a relative time sequence, the authors followed the methodology proposed, for example, by Nemčok *et al.* (1999), Kiss *et al.* (2001), and Sperner and Zweigel (2010).

Seismic data

The area of structural-data acquisition overlaps with that covered by a seismic profile (Fig. 6), perpendicular to the regional cross-section (Fig. 1). The seismic data were prestack depth migrated, but due to the lack of velocity information from deep boreholes, calibration was not performed. Thus, there is a depth mismatch between seismic horizons and corresponding geologic boundaries; the non-calibrated depth migrated data may overestimate the depth to geologic boundaries by 5–10%. To interpret the seismic section, the authors projected bedding-dip measurements from the surface onto the cross-section plane and used the available borehole data and the results from gravity and magnetic modelling to link seismic horizons with geological boundaries (Mikołajczak *et al.,* 2021). The interpretation of the seismic profile is based on the results of Barmuta *et al.* (2021) and Mikołajczak *et al.* (2021).

RESULTS

Cross-section

The cross-section shows the structure of the westernmost POC fold-and-thrust belt, the underlying sedimentary cover of the NEP, and the geometry of the top of the crystalline basement (Fig. 3). In the north, the crystalline basement is subhorizontal, constrained by borehole, gravity and magnetic data (Barmuta *et al.,* 2019; Mikołajczak *et al.,* 2021). The dip increases southward, reaching ca. 10° below the Magura

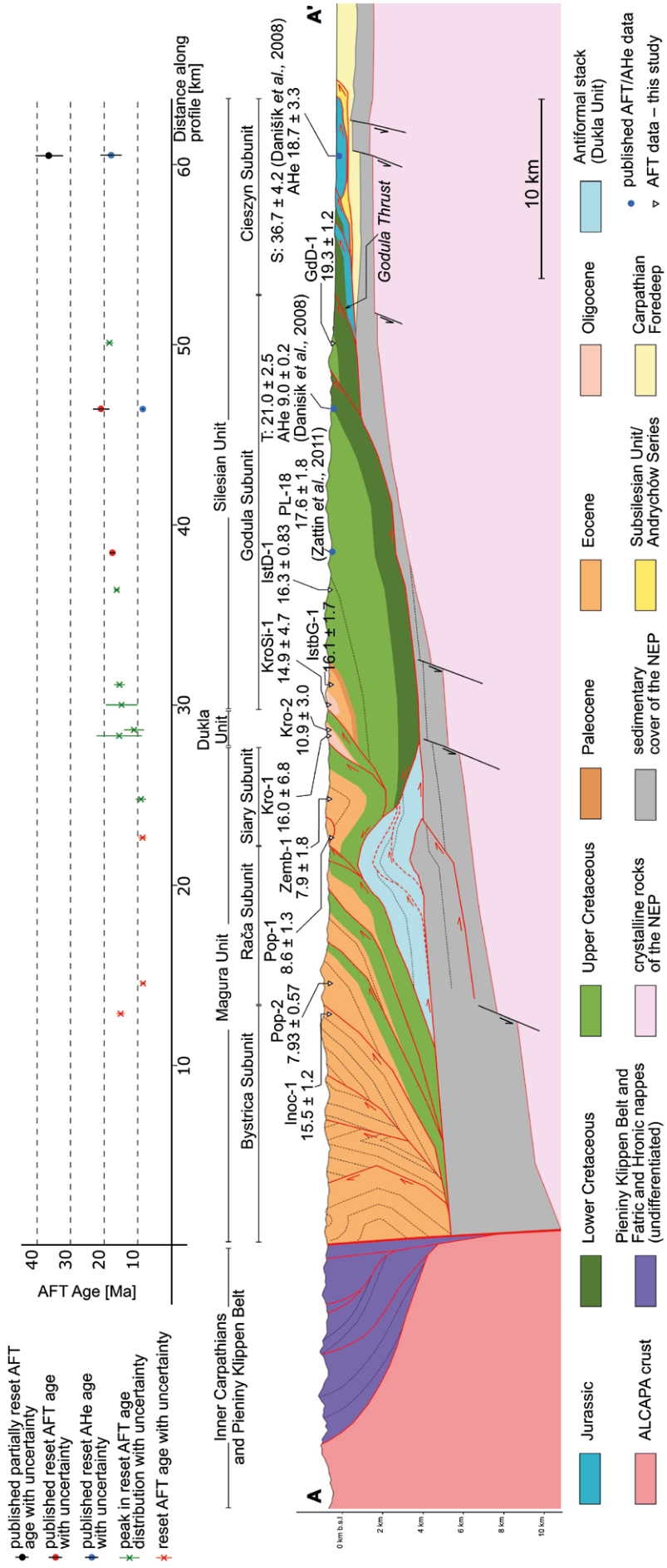

Fig. 3. Cross-section with the location and age of apatite fission-track samples. Modified after Barmuta *et al.* (2021). See text for details.

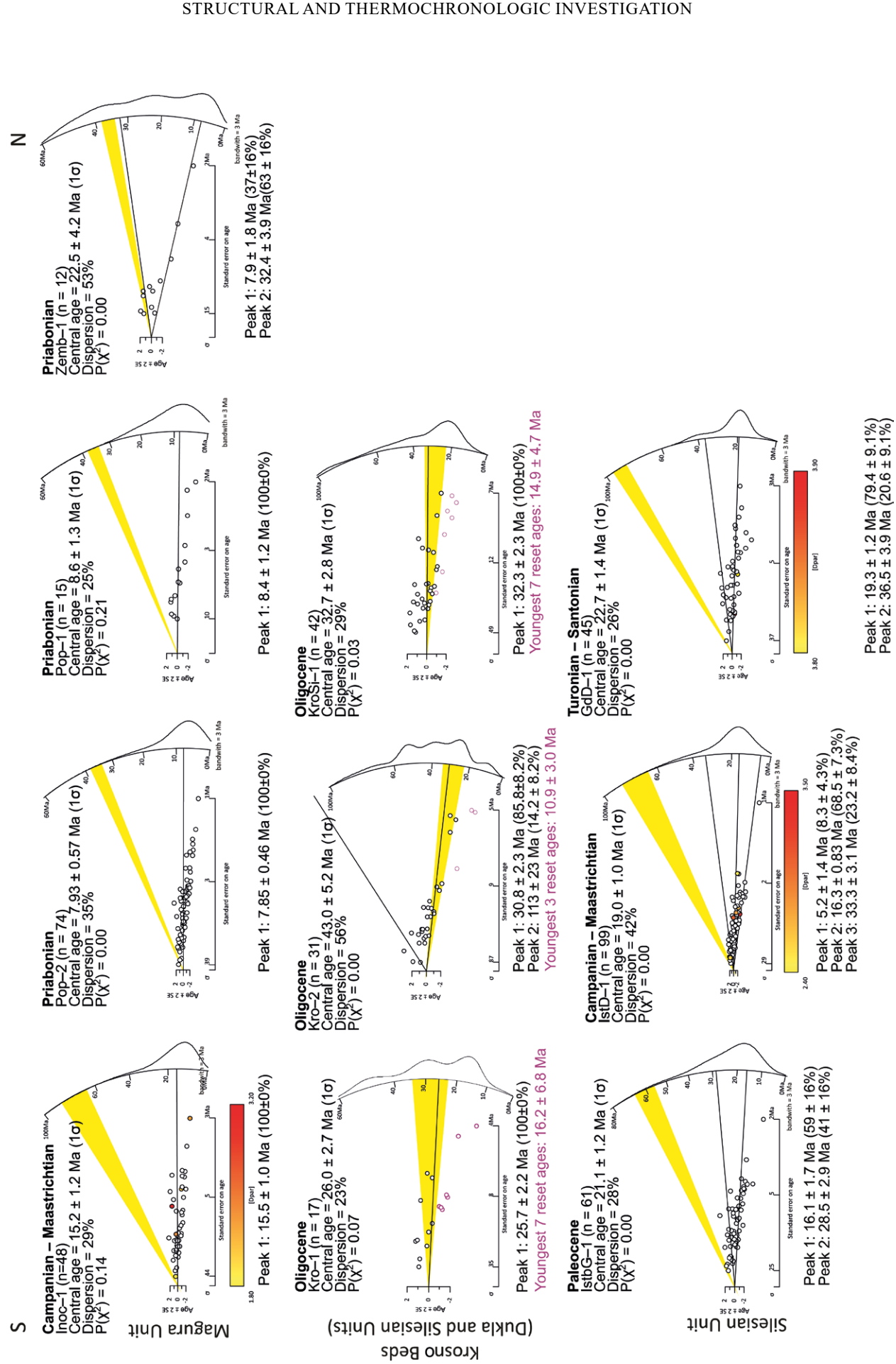

Fig. 4. Abanico plots for the apatite fission-track samples arranged by the samples' stratigraphic age and location from south to north in the respective units. The yellow polygons mark the stratigraphic age of each sample. For locations see Figures 1 and 3. See text for discussion.

Table 1

Apatite fission-track data with location of samples and preferred age interpretation.

Sample	Latitude (°N)	Longitude (°E)	Stratigraphic age (Ma)	N	N_s	N_i	$\sigma_{(Ns/Ni)\,(\%)}$	P[χ^2]%	Pooled ζ–age (±1s)	Central ζ–age (±1s)	$l_{m\ [\mu m]}$	S.D. $l_{m\ [\mu m]}$	l_c [µm]	S.D. $l_{c\ [\mu m]}$	N_{CT}	Dpar [µm]	Age peaks (2s, %); [Dispersion %]
Inoc-1	19.16090	49.44867	83.6–66.0	48	280	3608	7.8	14	15.5 ± 1.0	15.2 ± 1.2	11.7	2.8	13.52	1.81	12	2.36	15.5 ± 2.0 [29]
Pop-2	19.15356	49.46416	38.0–33.9	74	337	8584	3.9	0	7.9 ± 0.5	7.9 ± 0.6	14.6	1.8	15.46	1.19	19	2.13	7.9 ± 0.9 [35]
Pop-1	18.90103	49.50357	38.0–33.9	15	53	1263	4.2	21	8.4 ± 1.2	8.6 ± 1.3	n.a.	n.a.	n.a.	n.a.	n.a.	n.a.	8.4 ± 2.4 [25]
Zemb-1	19.00035	49.51416	38.0–33.9	12	119	1466	10.0	0	20.0 ± 1.0	22.5 ± 4.2	13.6	1.8	14.66	1.41	8	n.a.	7.9 ± 3.6 (37), 32.4 ± 7.8 (63) [53]
Kro-1	19.05507	49.57089	33.90–23.03	17	159	1236	1.4	7	25.7 ± 2.2	26.0 ± 2.7	n.a.	n.a.	n.a.	n.a.	n.a.	n.a.	25.7 ± 4.4 [18]
Kro-2	18.97491	49.54226	33.90–23.03	31	346	1862	18.6	0	37.1 ± 2.3	43.0 ± 5.2	11.6	2.7	13.97	1.14	4	n.a.	30.8 ± 4.6 (86), 113 ± 46 (14) [56]
KroSi-1	18.95487	49.55764	33.90–23.03	42	254	1569	16.2	3	32.3 ± 2.3	32.7 ± 2.8	n.a.	n.a.	n.a.	n.a.	n.a.	n.a.	32.3 ± 4.6 [29]
IstbG-1	19.00969	49.57662	66.0–56.0	61	672	6433	10.4	0	20.7 ± 0.9	21.1 ± 1.2	14.1	2.2	15.18	1.43	19	3.4	16.1 ± 3.4 (59), 28.5 ±5.8 (41) (28)
IstD-1	18.95090	49.61432	83.6–66.0	99	1370	15319	8.9	0	17.9 ± 0.6	19.0 ± 1.0	n.a.	n.a.	n.a.	n.a.	n.a.	2.9	5.2 ± 2.8 (8), 16.3 ± 1.6 (69), 33.3 ± 6.2 (23) [42]
GdD-1	18.81491	49.70036	93.9–83.6	45	646	5734	11.3	0	22.5 ± 1.0	22.7 ± 1.4	15.1	1.7	15.51	1.33	29	3.7	19.3 ± 2.4 (79), 36.5 ± 7.8 (21) [26]

Notes: Analyst – Saeideh Asal Seyedi with ζ-calibration factor of 276 ± 5 yr cm² (± 1s) determined on Durango and Fish Canyon Tuff apatite age standards and IRMM 540R dosimeter glass; N – number of counted grids (= grain number); N_s, N_i – number of spontaneous and induced fission tracks, respectively; – unweighted standard error of the ratio between spontaneous and induced tracks; – chi-square test to statistically test the null-hypothesis that the analysed grains belong to one age population, ≥5% one age population; – track density of co-irradiated dosimeter glass (IRMM 540R), 1.45 (10^6 cm^{-2}) ± 1.32 (10^4 cm^{-2}, 1s); l_m – mean track length of measured confined fission tracks; l_c – mean c-axis-projected track length of measured confined fission tracks; S.D. – standard deviation; N_{CT} – number of measured confined fission tracks; Dpar – maximum diameter of the fission-track etch figure parallel to the grain c-axis; Age peaks – peaks in the grain-age distribution calculated by RadialPlotter, () – % of grains building the age peak; Dispersion – dispersion of single-grain ages; n.a. – analysis not possible due to lack of data. Ages in million years (Ma).

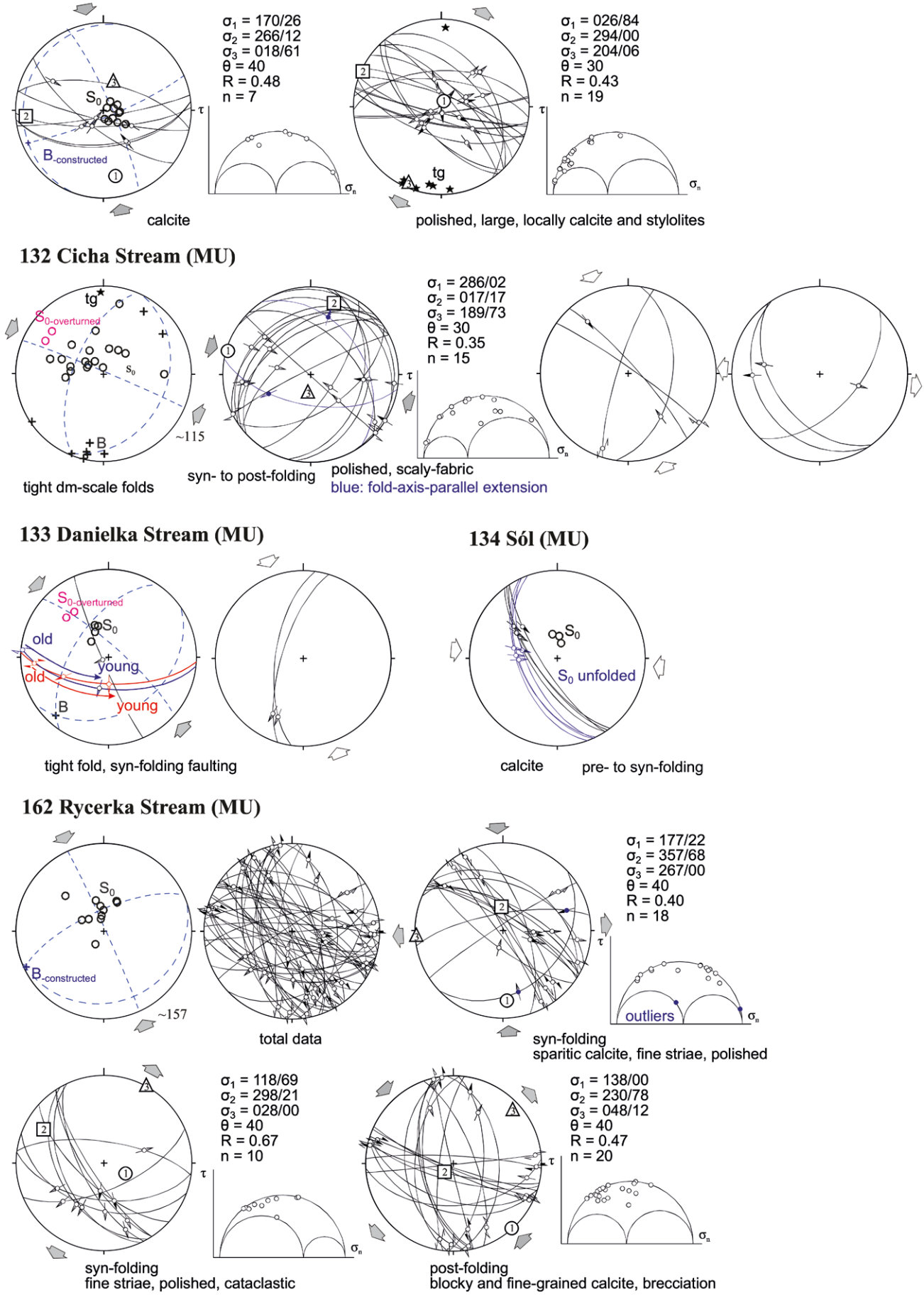
131 Glinka Quarry (MU)
S0
B-constructed
σ1 = 170/26
σ2 = 266/12
σ3 = 018/61
θ = 40
R = 0.48
n = 7
calcite
tg
σ1 = 026/84
σ2 = 294/00
σ3 = 204/06
θ = 30
R = 0.43
n = 19
polished, large, locally calcite and stylolites
132 Cicha Stream (MU)
tg
S0-overturned
s0
B
~115
tight dm-scale folds
σ1 = 286/02
σ2 = 017/17
σ3 = 189/73
θ = 30
R = 0.35
n = 15
syn- to post-folding
polished, scaly-fabric
blue: fold-axis-parallel extension
133 Danielka Stream (MU)
S0-overturned
S0
old
young
old
young
B
tight fold, syn-folding faulting
134 Sól (MU)
S0
S0 unfolded
calcite
pre- to syn-folding
162 Rycerka Stream (MU)
S0
B-constructed
~157
total data
σ1 = 177/22
σ2 = 357/68
σ3 = 267/00
θ = 40
R = 0.40
n = 18
outliers
syn-folding
sparitic calcite, fine striae, polished
σ1 = 118/69
σ2 = 298/21
σ3 = 028/00
θ = 40
R = 0.67
n = 10
syn-folding
fine striae, polished, cataclastic
σ1 = 138/00
σ2 = 230/78
σ3 = 048/12
θ = 40
R = 0.47
n = 20
post-folding
blocky and fine-grained calcite, brecciation

Fig. 5

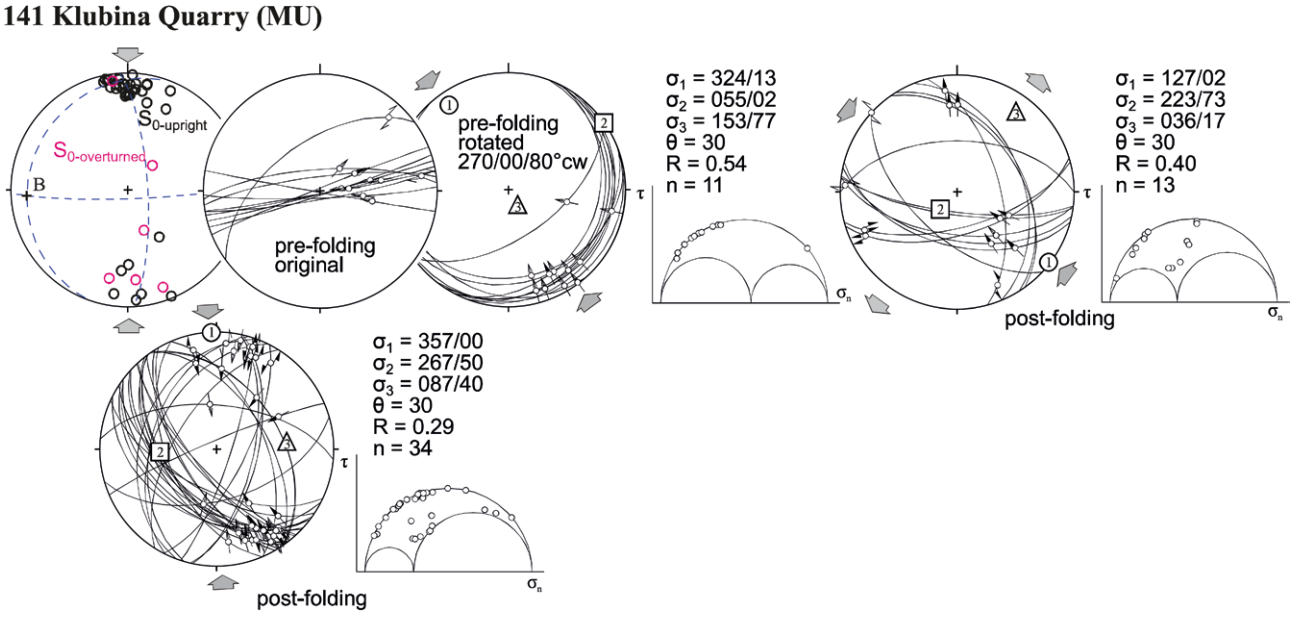

Fig. 5. Schmidt's lower hemisphere stereonet plots for structural data measured in selected outcrops in the Magura Unit (for locations see Figure 1). Arrows around the plots indicate subhorizontal maximum and minimum stress orientation determined from fault-striae analysis or cylindrical fold orientation (filled arrows, calculated; open arrows, estimated). Faults are drawn as great circles and slip directions along striae as arrows pointing in the direction of the displacement of the hanging wall. Confidence levels of slip-sense determination are expressed in the arrowhead style: solid, certain; open, reliable; half, unreliable; without head, poor. Reduced stress-tensor calculations: principal stress orientations (σ_{1}–$_{3}$); θ, fracture angle used for calculation; R, shape factor of stress-ellipsoid = $(\sigma_2–\sigma_3)/(\sigma_1–\sigma_3)$; n, number of data used for calculation; dimensionless Mohr diagram visualizes normal versus shear stress relationships for each fault (circles). Abbreviations: B, fold axis; s_0, bedding; tg, tension gash.

Table 2

Outcrops investigated by structural analysis. MU – Magura Unit.

No	Outcrop Number	Name	Lithostratigraphy	Unit	Latitude WGS84	Longitude WGS84
1	131	Glinka Quarry	Magura Formation	MU	49.4641°N	19.15304°E
2	132	Cicha Stream	Beloveža Formation. Eocene	MU	49.45259°N	19.14557°E
5	141	Klubina Quarry	Magura Formation. Eocene	MU	49.36413°N	18.8965°E
6	161/162	Rycerka Stream	Szczawina Sandstone Formation. Campanian–Maastrichtian	MU	49.45923°N	19.06986°E
11	133	Danielka Stream	Magura Formation. Eocene–Oligocene	MU	49.43803°N	19.10057°E
12	134	Sól	Magura Formation. Eocene–Oligocene	MU	49.49405°N	19.05318°E

Unit. In the southern part, normal faults with 600–900 m throw form a stair-step geometry, as indicated by the joint interpretation of gravity and magnetic data (Mikołajczak *et al.,* 2021). The sedimentary cover above the crystalline basement is poorly constrained lithostratigraphically. Sparse data from the Czech Republic (Blizkovsky *et al.,* 1994; Picha *et al.,* 2006) and Poland (Florek *et al.,* 1998; Wójcik and Nescieruk, 2000; Nescieruk and Wójcik, 2001) suggest that most of it comprises Devonian–Carboniferous clastic and carbonate rocks. The thickness of the sedimentary cover increases from hundreds of metres in the north to up to 5 km in the south (Fig. 3), where its thickness was estimated based on the integrated interpretation of seismic, gravity and magnetic methods (Barmuta *et al.,* 2019; Mikołajczak *et al.,* 2021).

In the northern part of the cross-section, the Miocene foredeep deposits were interpreted to extend below the frontal thrust. These Miocene strata were subdivided into an autochthonous part and the allochthonous Andrychów Unit, which comprises olistoliths, derived from the inner OC (e.g., Wójcik and Jugowiec, 1998; Wójcik *et al.,* 2001; Połtowicz, 2004). The few boreholes that penetrated the inner POC fold-and-thrust belt do not constrain the southern extent of the allochthonous Miocene strata below the fold-and-thrust belt. However, the Jablunkov-1 borehole in the Czech Republic (Picha *et al.,* 2006), the Bystra-IGl borehole

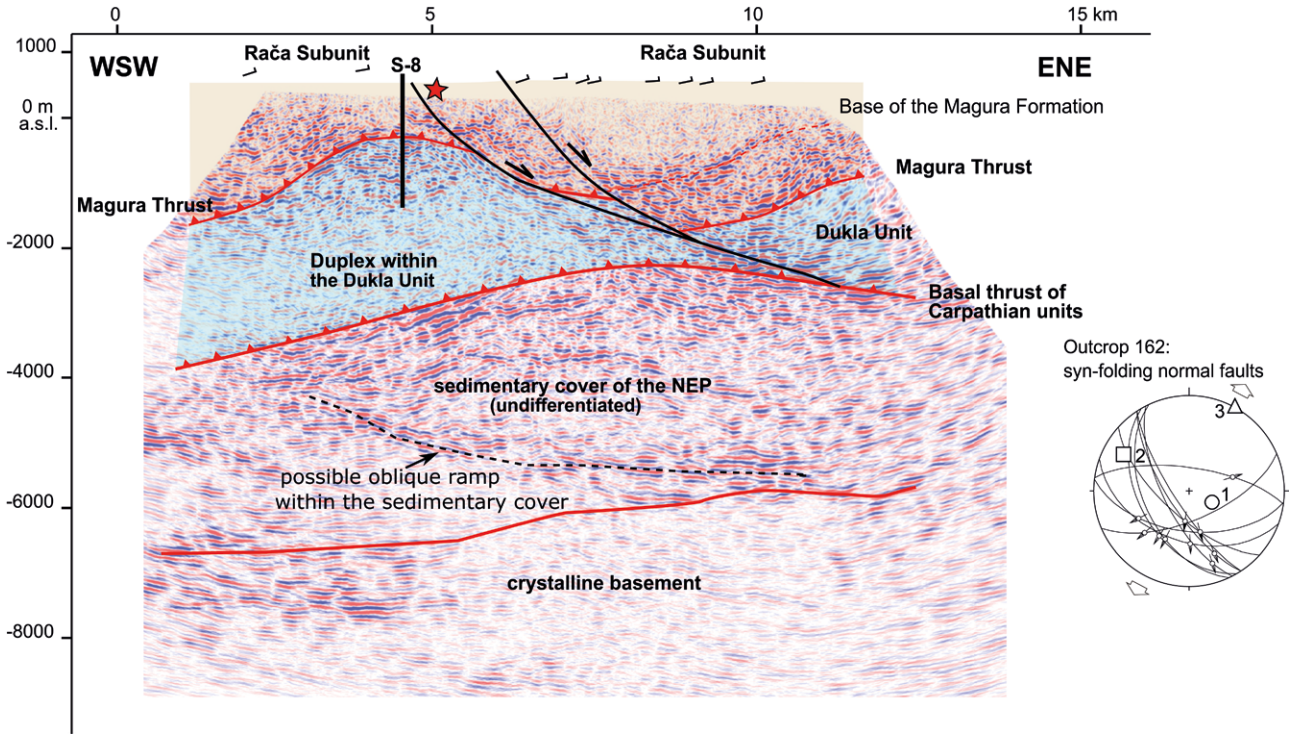

Fig. 6. Strike-parallel seismic section (for location see Figure 1) showing normal faults developed along the eastern lateral wall of the Dukla Unit antiformal stack. Stereonet plot illustrates NE–SW extension determined from outcrop data, which records a fault set antithetic to the major normal fault structure imaged by the seismic data. The position of the outcrop is marked with a red star. S-8 – Sól-8 borehole. Seismic section interpretation modified after Barmuta *et al.* (2021).

(Fig. 1), and the Zawoja-IG1 borehole, located to the east of the area shown in Figure 1 (Gedl, 1997; Oszczypko, 1997), suggest that Miocene strata may in part underlie the Magura Unit. As the Miocene was not encountered in all boreholes penetrating the Carpathian substratum, the authors assume that it forms isolated patches rather than a continuous layer. Because the Andrychów Unit is equivocally defined and not clearly separated from the Subsilesian Unit and their combined thickness is insignificant at the scale of cross-section, the authors do not show them in Figure 3. The basal thrust of the POC fold-and-thrust belt maintains a constant southward dip of ca. 4°.

The structure of the fold-and-thrust belt is bipartite. The northern part comprises the Silesian Unit divided into the Cieszyn and Godula subunits. The uppermost Jurassic and Lower Cretaceous strata of the Cieszyn Subunit are stacked into narrow, foreland-vergent thrust sheets. South of the Godula Thrust (Figs 1, 3), the Godula Subunit forms a homocline, consisting of a continuous, Upper Cretaceous to Oligocene, sandstone-dominated sequence. Whether Upper Jurassic strata occur at the base of the Godula Unit is unclear, due to the lack of seismic and borehole data. South of the Silesian Unit and the narrow zone of the Dukla Unit, the Magura Unit consists of a stack of thrust sheets. The presence of an antiformal stack below the northern part of the Magura Unit (Barmuta *et al.,* 2021) is inferred from the seismically-imaged geometry of the Magura sole thrust; its concave-upward shape is interpreted as evidence for the stack. While the skeleton of the antiformal stack can be inferred from the seismic data, its poor internal reflectivity does not allow the interpretation of its geometry, i.e., the number of imbricates and the related thrust displacements. The position of the antiformal stack coincides with a thrust-related topographic high in the sedimentary cover of NEP, which may reflect the presence of a hanging-wall anticline above a thrust ramp (Fig. 3).

Apatite fission-track dating results

The AFT ages show significant dispersion (Tab. 1; Fig. 4). This reflects their origin from detrital rocks, the source rocks of which probably varied in age and chemical composition, the different transport processes from source to sink, and the variable thermal overprint of the apatites due to burial that reset the original detrital ages to different degrees. This also affects the number of countable grains (12–99; Tab. 1) and the abundance of countable prism faces that determine the number of Dpar data. Both the low number of apatite grains and the young ages do not allow for a sufficient number of confined track measurements to perform temperature-time modelling at this reconnaissance stage of thermochronologic investigation (Tab. 1). Increasing the number of confined tracks that are etched and can be measured will need sophisticated methods, such as ion irradiation (Min *et al.,* 2007). Figure 3 shows the published and new AFT and AHe ages, projected onto the cross-section; here, the authors use the central AFT ages, as the best representation of heterogeneous data. The top panel of Figure 3 shows

the ages, subdividing the data into reset ages, partially-rest ages, and ages that represent the major peak in the reset age distribution. Figure 3 (the cross-section) and Figure 4 (the Abanico plots) show some common features. (1) All pre-Oligocene samples of the Silesian Unit (represented by samples IstbG-1, IstD-1, and GdD-1) have AFT single-grain ages that are in general younger than the depositional ages, thus their ages are mostly reset. However, the age distribution of these samples shows age peaks (Tab. 1). The ages of the major peaks overlap with the probably reset ages of Zattin *et al.,* (2011; their sample PL-18) and Danišík *et al.,* (2008; their sample T) but are much younger than the age of sample S of Danišík *et al.,* (2008) from the Cieszyn Subunit. The ages of the present study overlap or are older than the two AHe ages of Danišík *et al.,* (2008). (2) The Oligocene rocks of the Krosno Beds (samples Kro-1, Kro-2, KroSi-1) from the Dukla and Silesian units have single-grain ages that are exclusively partially reset, mostly overlapping with the depositional age; they have some grains younger than the depositional age (Tab. 1). (3) The ages from the Magura Unit are reset (samples Inoc-1, Pop-1, Pop-2) or partially reset (sample Zemb-1; Tab. 1); the latter has a distinct young peak of the reset ages, overlapping with the other ages.

Structural data

The time-sequence relationships allowed the authors to split the data into pre-, syn-, and post-folding phases of deformation. Pre-folding fault-striae sets are characterized by an association with folded bedding, with early-formed faults, often rotated into apparent normal faults (e.g., pre-folding set in station 141, Fig. 5); upon unfolding by the measured bedding dips, the sets display thrust or strike-slip solutions. Syn-folding sets usually represent slip along dipping bedding surfaces or conjugate fault sets with variable fault dips and striae plunges, indicating formation during progressive folding (e.g., syn-folding set in station 162, Fig. 5). Post-folding faults cut the folds and faults, formed in the earlier stages; in general, they have subhorizontal striae (e.g., post-folding set in station 162, Fig. 5). In the studied outcrops, conjugate strike-slip fault sets are most common, subordinate are thrust-fault sets; normal faults are least abundant.

The structural data (Fig. 5) mostly comprise tight, locally overturned folds formed under NW–SE to N–S shortening and pre-, syn-, and post-folding fault-striae sets with σ_1 (maximum compression) trends that correspond to the shortening directions, derived from the mostly cylindrical folds. These data were observed throughout the Magura Unit regardless of the stratigraphic age of the studied rocks (Figs 2, 5). The authors did not observe the Middle–Late Miocene top-to-NNE thrusting and sinistral strike-slip faulting, related to the eastern Alpine extrusion tectonics (Ratschbacher *et al.,* 1991a, b; Fodor, 1995), post-dating the earlier compression phase, and described farther southwest in the OC of the Czech Republic by Beidinger and Decker (2016). In addition, the present authors did not detect the post-thrusting, arc-orthogonal extension. In some outcrops, the authors observed the syn- to post-folding fault-striae sets with normal and transtensional faults striking orthogonal to the map–scale thrusts and folds (Figs 5, 6). Seismic investigations (Barmuta *et al.,* 2021) probably show the dimensions of these structures, cutting locally most of the fold-and-thrust belt (Fig. 6).

DISCUSSION

As the cross-section in the present study runs parallel to the tectonic transport direction, a preliminary estimate of the amount of shortening can be given. The presently-known southern extent of the Miocene foredeep-basin strata yields a minimum of 40 km of horizontal displacement of the whole pile of Carpathian units (Picha and Stráník, 1999), as also suggested by the Jablunkov-1 borehole (Fig. 1), which encountered Miocene strata below the basal thrust of the Carpathians (Picha *et al.*, 2006). The present-day N–S extent of the Silesian Unit is ca. 35 km. On the basis of the ramp geometry of the Godula Thrust and the partially-reset to reset AFT ages and the reset AHe ages in its hanging wall, the present authors suggest a minimum of 10 km of horizontal displacement. Thus, the minimum shortening for the Silesian Unit is ≥50 km. The complicated internal structure of the Magura Unit makes shortening estimates challenging, especially due to the lack of borehole and geophysical data from the Slovakian part of the Bystrica Subunit, which would be paramount to constraining the subsurface structural geometry. The authors used the pre-deformed, ca. 64 km width estimate for the Magura Basin from the profile balanced by Nemčok *et al.,* (2001), located ca. 50 km to the east of the studied area. When compared with the present-day width of the Magura Unit in the cross-section of the present study (ca. 30 km), a value of ca. 50% of shortening is obtained, fitting the structural style. The initial width of the Silesian, Magura, and foredeep units is thus ≥110 km.

The initial length of the Dukla Unit in front of the Magura Unit and within the antiformal stack is also difficult to estimate; a better seismic resolution is necessary. Using the interpretation shown in Figure 3, the authors speculate about an initial length ca. 17 km initial length. Summarizing, the initial width of the POC basins is at least 130 km, which is close to the ca. 135 km estimate of Castelluccio *et al.* (2016) for the central POC thrust-and-fold belt and the ca. 195 km, provided by Nemčok *et al.* (2001). These estimates support a general trend of eastwardly increasing bulk shortening along the OC fold-and-thrust belt.

Similar structures (Fig. 5; folds and fault-striae sets) and NW–SE to N–S shortening directions were observed throughout the Magura Unit, regardless of the stratigraphic age of the studied rocks. This suggests that the observed deformation is younger than the age of the youngest studied strata, i.e., the Eocene Zembrzyce Beds. This agrees with the regional-scale evolution of the deformation field from the Oligocene to the middle Badenian (a Central Paratethys stage, roughly equivalent to the Langhian and lower Serravallian; Fodor, 1995; Nemčok *et al.,* 2007; Beidinger and Decker, 2016; Márton, 2020). The present authors attribute the lack of the Middle–Late Miocene top-to-NNE thrusting and sinistral strike-slip faulting related to the eastern Alpine extrusion tectonics (e.g., Ratschbacher *et*

al., 1991a) in the studied area to its progressive fading out towards the outer parts of the POC fold-and-thrust belt; it also has not been observed in the central and eastern POC (Rubinkiewicz, 2000, 2007; Nemčok *et al.,* 2007). That the present authors did not detect the post-thrusting, arc-orthogonal extension supports the observation of Mazzoli *et al.* (2010) and Zattin *et al.,* (2011) that these structures formed only in the central and eastern POC. On the other hand, the present authors observed syn- to post-folding fault-striae sets with normal and transtensional faults striking orthogonal to the map-scale thrusts and folds (Figs 5, 6). The authors interpret these structures as formed by along-strike extension, related to the adjustment of the fold-and-thrust belt to the oroclinal shape of the foreland, imposing fold axis-parallel extension. The seismic investigations of Barmuta *et al.* (2021) suggest that these faults cut large portions of the fold-and-thrust belt (Fig. 6).

In the northern Silesian Unit and the Cieszyn Subunit, Danišík *et al.* (2008) interpreted their AFT (36.7 ± 4.2 Ma) and AHe (18.7 ± 3.3 Ma) ages (sample S; Figs 1, 3) as indicating that exhumation started in the Eocene and lasted till the Miocene. The authors presume that the AFT age of this Cretaceous teschenite sample was partially reset (the 1σ uncertainty is 4.2 Ma), thus that it is not geologically meaningful. The AHe age overlaps within uncertainty with the reset AFT ages and age peaks of the southerly-abutting Godula Subunit samples. Interpreted in the context of shortening-related exhumation, this indicates an Early Miocene onset of thrusting and exhumation.

The southern part of the Silesian Unit, i.e., the Godula Subunit, shows within the range of error an identical reset or reset peak of AFT ages (16.1–17.6 Ma; Fig. 3; Tab. 1), compatible with its gently southward-dipping homocline geometry. Sample GdD1 in the footwall of the Godula Thrust is nearly reset with a major peak of reset ages at ca. 19.3 Ma, supporting that a ca. E-striking thrust divides the Godula Subunit into two sheets (Figs 1, 3). Sample T with a ca. 21.0 Ma AFT age (Danišík et al., 2008) just above this thrust supports its presence but due to the large projection distance (>40 km, Fig. 1), its position on the cross-section plane is tentative.

The authors interpret the reset (7.9–15.2 Ma; average ca. 10 Ma) AFT ages from the Magura Unit as evidence for a second, younger exhumation phase (Nemčok *et al.,* 1998b, 2001; Świerczewska and Tokarski, 1998; Świerczewska, 2005; Anczkiewicz and Świerczewska, 2008; Cieszkowski *et al.,* 2009; Oszczypko and Oszczypko–Clowes, 2009). These AFT ages correspond to ages from the eastern POC fold-and-thrust belt (Mazzoli *et al.,* 2010; Zattin *et al.,* 2011), which were interpreted as an effect of post-thrusting, arc-orthogonal extension. Due to the lack of structural evidence for this deformation in the western POC fold-and-thrust belt, the authors propose alternative interpretations. First, the Late Miocene ages are linked to the formation of the antiformal stack of the Dukla Unit beneath the Magura Unit. This interpretation is supported by the observation that the stack formed after the deposition of the Oligocene Krosno Beds of the Dukla Unit, as inferred from the deformation of the basal thrusts of the Magura and Dukla units (Barmuta *et al.,* 2021); the post-Oligocene formation emphasizes the out-of-sequence character of the antiformal stack. Late, out-of-sequence underthrusting of the Magura Unit was already proposed by Fodor (1991, 1995) and Świerczewska (2005) and is supported by the studies in the Ukrainian Carpathians (Nakapelyukh *et al.,* 2018; Roger *et al.,* 2023), where out-of-sequence duplexing was also suggested on the basis of thermochronologic studies, cross-section balancing, and structural forward modelling. Late Miocene (ca. 9 Ma) deformation of foredeep deposits in the western part of POC fold-and-thrust belt, east of the map of Figure 1 (Wójcik and Jugowiec, 1998), also supports a Late Miocene adjustment of the accretionary wedge, post-dating the main thrusting phase. The formation of the antiformal stack implies ca. 2.5 km of exhumation above its apex, probably causing the Late Miocene AFT ages.

The second interpretation of the present authors for the Late Miocene AFT ages relates these to the arc-parallel extension, documented by thrust-orthogonal normal faults (Fig. 5). Such faults were documented at the surface (Fig. 1; Burtan *et al.,* 1973; Fodor, 1991; Ryłko *et al.,* 1992, 1993; Starzec *et al.,* 2014; Ryłko, 2018), in seismic sections (Fig. 6; Barmuta *et al.,* 2021), and in the studied outcrops (Fig. 5). The seismic interpretation suggests that the throw may reach ca. 2 km (Fig. 6).

The third and preferred interpretation of the present authors for the young AFT ages is that antiformal stack formation and along-strike extension interacted. It is striking that the antiformal stack of the Dukla Unit is located in the footwall of the seismically imaged thrust-orthogonal normal fault (Fig. 6). The duplex formation may have focused extension along its lateral culmination wall, forming a hanging-wall drop fault *sensu* Butler (1982); such a lateral culmination wall favours the formation of arc-orthogonal normal faults.

On the basis of the cross-section and the reconnaissance AFT results, the authors can speculate on the exhumation rates. The estimation of these rates depends on the assumed paleo-geothermal gradient. Illite-smectite and fluid inclusion studies in the POC fold-and-thrust belt suggest a variation in time and space from 17 to 29 °C/km (Świerczewska, 2005; Hurai *et al.,* 2006; Roger *et al.,* 2023). Using an average value of 20 °C/km and interpreting the ages of samples Pop-1, Pop-2, and Zemb-1 as reset, the authors postulate that ≥5 km of overburden was removed during the imbrication of the Magura Unit. The authors infer a lower value of exhumation for the Silesian and Dukla units: the partially-reset AFT ages from the Krosno Beds indicate exhumation from depths within the AFT partial-annealing zone (100–60 °C; e.g., Gleadow *et al.,* 1986). The two published, probably reset AHe ages, indicate exhumation from below the AHe partial retention zone (ca. 80–40 °C; Farley, 2000). Thus, about 4–2 km of overburden was removed from the Silesian and Dukla units.

CONCLUSIONS

The northward younging of the stratigraphic age of the syn-tectonic formations, i.e., from the Magura Formation over the Zembrzyce Beds to the Krosno Beds, suggests in-sequence stacking of the fold-and-thrust belt, commencing in the Eocene in the Magura Unit and lasting until the

Oligocene/Miocene in the Dukla and Silesian units. On the basis of published and new reconnaissance AFT ages and the published AHe ages, the present authors infer that thrusting in the Silesian Unit commenced in the Early Miocene (≤20 Ma). The Late Miocene AFT ages across the northern part of the Magura Unit suggest a phase of out-of-sequence thrusting in the hinterland part of the POC fold-and-thrust belt. This interpretation fits the tectonic evolution, proposed for the eastern POC and the Ukrainian OC fold-and-thrust belts. The authors relate the out-of-sequence thrusting and the ensuing Late Miocene AFT ages to the interaction of convergence-parallel shortening, that formed the antiformal stack of the Dukla Unit below the Magura Unit, and the along-strike extension that caused a hanging-wall drop fault. The present structural study does not support post-thrusting, arc-orthogonal extension in the western part of the POC fold-and-thrust belt. Consequently, post-stacking collapse of the fold-and-thrust belt cannot be regarded as a key factor inducing the young (ca. 10 Ma) exhumation, as stated for the eastern sector of the POC fold-and-thrust belt. The present interpretation implies the necessity of additional AFT and AHe dating for validation in the western POC fold-and-thrust belt.

Acknowledgments

The research was supported by the Miniatura 7 Grant of the Polish National Science Centre: "Thermochronological investigations in Outer Carpathians west of Żywiec", granted to Jan Barmuta, and Statutory Funds 16.16.140.315/05 of the Department of Energy Resources of the Faculty of Geology, Geophysics and Environmental Protection, AGH University of Kraków. We also acknowledge the use of the Move Software by Petex LTD, granted to the AGH University of Kraków. We would like to thank L. Fodor and an anonymous reviewer for their constructive comments, which significantly improved the manuscript. We also acknowledge the support of the Editors.

REFERENCES

Abdulhameed, S., Ratschbacher, L., Jonckheere, R., Gągała, Ł., Enkelmann, E., Käßner, A., Kars, M. A. C., Szulc, A., Kufner, S. K., Schurr, B., Ringenbach, J. C., Nakapelyukh, M., Khan, J., Gadoev, M. & Oimahmadov, I., 2020. Tajik basin and southwestern Tian Shan, northwestern India-Asia collision zone: 2. Timing of basin inversion, Tian Shan mountain building, and relation to Pamir Plateau advance and deep India-Asia indentation. *Tectonics*, 39: 1–26.

Anczkiewicz, A. A. & Świerczewska, A., 2008. Thermal history and exhumation of the Polish Western Outer Carpathians: evidence from combined apatite fission track and illite - smectite data. In: Garver, J. I & Montario, M. J. (eds), *FT2008, Abstract Book of the 11th International Conference on Thermochronology*, *Anchorage Alaska, September 2008,* pp. 1–4.

Andreucci, B., Castelluccio, A., Corrado, S., Jankowski, L., Mazzoli, S., Szaniawski, R. & Zattin, M., 2014. Interplay between the thermal evolution of an orogenic wedge and its retro-wedge basin: An example from the Ukrainian Carpathians. *Bulletin of the Geological Society of America*, 127: 410–427.

Andreucci, B., Castelluccio, A., Jankowski, L., Mazzoli, S., Szaniawski, R. & Zattin, M., 2013. Burial and exhumation history of the Polish Outer Carpathians: Discriminating the role of thrusting and post-thrusting extension. *Tectonophysics*, 608: 866–883.

Angelier, J., 1984. Tectonic analysis of fault slip data sets. *Journal of Geophysical Research: Solid Earth*, 89(B7): 5835–5848.

Barmuta, J., Mikołajczak, M. & Starzec, K., 2019. Constraining depth and architecture of the crystalline basement based on potential field analysis – the westernmost Polish Outer Carpathians. *Journal of Geosciences (Czech Republic)*, 64: 161–177.

Barmuta, J., Starzec, K. & Schnabel, W., 2021. Seismic-scale evidence of thrust-perpendicular normal faulting in the western Outer Carpathians, Poland. *Minerals*, 11: 1–26.

Behrmann, J. H., Stiasny, S., Milicka, J. & Pereszlenyi, M., 2000. Quantitative reconstruction of orogenic convergence in the northeast Carpathians. *Tectonophysics*, 319: 111–127.

Beidinger, A. & Decker, K., 2016. Paleogene and Neogene kinematics of the Alpine-Carpathian fold-thrust belt at the Alpine-Carpathian transition. *Tectonophysics*, 690: 263–287.

Blizkovsky, M., Kocak, A., Morkovsky, M. & Novotny, A., 1994. Exploration history, geology and hydrocarbon potential in the Czech Republic and Slovakia. In: Popescu, B. M. (ed.), *Hydrocarbons of Eastern Central Europe: Habitat, Exploration and Production.* Springer Berlin, Heidelberg, pp. 71–117.

Brückl, E., Behm, M., Decker, K., Grad, M., Guterch, A., Keller, G. R. & Thybo, H., 2010. Crustal structure and active tectonics in the Eastern Alps. *Tectonics*, 29: 1–17

Buford Parks, V. M. & McQuarrie, N., 2019. Kinematic, flexural, and thermal modelling in the Central Andes: Unravelling age and signal of deformation, exhumation, and uplift. *Tectonophysics*, 766: 302–325.

Burtan, J., Nescieruk, P. & Wójcik, A., 1973. *Szczegółowa Mapa Geologiczna Polski w skali 1: 50 000, arkusz Wisła (1028)*. Wydawnictwa Geologiczne, Warszawa. [In Polish.]

Burtan, J., Paul, Z. & Watycha, L., 1978. *Szczegółowa Mapa Geologiczna Polski, skala 1:50 000, arkusz Mszana Górna (1033)*. Wydawnictwa Geologiczne, Warszawa. [In Polish.]

Burtner, R. L., Nigrini, A. & Donelick, R. A., 1994. Thermochronology of Lower Cretaceous source rocks in the Idaho-Wyoming thrust belt. *AAPG Bulletin,* 78: 1613–1636.

Butler, R. W. H., 1982. The terminology of structures in thrust belts. *Journal of Structural Geology*, 4: 239–245.

Carlson, W. D., Donelick, R. A. & Ketcham, R. A., 1999. Variability of apatite fission-track annealing kinetics: I. Experimental results. *American Mineralogist*, 84: 1213–1223.

Castelluccio, A., Andreucci, B., Zattin, M., Ketcham, R. A., Jankowski, L., Mazzoli, S. & Szaniawski, R., 2015. Coupling sequential restoration of balanced cross sections and low-temperature thermochronometry: The case study of the Western Carpathians. *Lithosphere*, 7: 367–378.

Castelluccio, A., Mazzoli, S., Andreucci, B., Jankowski, L., Szaniawski, R. & Zattin, M., 2016. Building and exhumation of the Western Carpathians: New constraints from sequentially restored, balanced cross sections integrated with low-temperature thermochronometry. *Tectonics*, 35: 2698–2733.

Central Geological Database 2024. Polish Geological Institute. http://baza.pgi.gov.pl/ [11.02. 2024].

Cieszkowski, M., Golonka, J., Krobicki, M., Ślączka, A., Oszczypko, N., Waśkowska, A. & Wendorff, M., 2009. The Northern Carpathians plate tectonic evolutionary stages and origin of olistoliths and olistostromes. *Geodinamica Acta*, 22: 101–126.

Cieszkowski, M., Golonka, J., Waśkowska-Oliwa, A. & Chodyń, R., 2007. Type locality of the Mutne Sandstone Member of the Jaworzynka Formation, Western Outer Carpathians, Poland. *Annales Societatis Geologorum Poloniae*, 77: 269–290.

Cohen, K. M., Finney, S. C., Gibbard, P. L. & Fan, J.-X., 2013. The ICS international chronostratigraphic chart. *Episodes Journal of International Geoscience*, 36: 199–204.

Danišík, M., Pánek, T., Matýsek, D., Dunkl, I. & Frisch, W., 2008. Apatite fission track and (U-Th)/He dating of teschenite intrusions gives time constraints on accretionary processes and development of planation surfaces in the outer Western Carpathians. *Zeitschrift für Geomorphologie*, 52: 273–289.

Dietze, M., Kreutzer, S., Burow, C., Fuchs, M. C., Fischer, M. & Schmidt, C., 2016. The Abanico plot: Visualising chronometric data with individual standard errors. *Quaternary Geochronology*, 31: 12–18.

Elias, M., 1992. Sedimentology of the Klentnice formation and the Ernstbrunn limestone (Zdanice-Subsilesian unit of the Outer West Carpathians). *Věstník Ústředního Ústavu Geologického*, 67: 179–193.

Farley, K., 2000. Helium diffusion from apatite: General behaviour as illustrated by Durango fluorapatite. *Journal of Geophysical Research*, 105(B2): 2903–2914.

Florek, R., Jawor, E., Pieniążek, I. & Zacharski, J., 1998. Możliwości akumulacji węglowodorów w utworach paleozoicznych w rejonie Andrychowa (Karpaty Zachodnie). *Nafta-Gaz*, 54: 428–439. [In Polish.]

Fodor, L., 1991. *Evolution tectonique et paléo-champs de contraintes soligocènes à quaternaires de la zone de transition Alpes orientales-Carpathes occidentales: formation et développement des bassins de Vienne et Nord pannoniens*. Unpublished Ph.D. Thesis, Université Paris VI Pierre-and-Marie-Curie University, 199 pp.

Fodor, L., 1995. From transpression to transtension: Oligocene–Miocene structural evolution of the Vienna basin and the East Alpine-Western Carpathian junction. *Tectonophysics*, 242: 151–182.

Gągała, Ł., Ratschbacher, L., Ringenbach, J. C., Kufner, S. K., Schurr, B., Dedow, R., Abdulhameed, S., Le Garzic, E., Gadoev, M. & Oimahmadov, I., 2020. Tajik basin and southwestern Tian Shan, northwestern India-Asia collision zone: 1. Structure, kinematics, and salt tectonics in the Tajik fold-and-thrust belt of the western foreland of the Pamir. *Tectonics*, 39: 1–32.

Gągała, Ł., Vergés, J., Saura, E., Malata, T., Ringenbach, J. C., Werner, P. & Krzywiec, P., 2012. Architecture and orogenic evolution of the northeastern Outer Carpathians from cross-section balancing and forward modeling. *Tectonophysics*, 532–535: 223–241.

Galbraith, R. F., 1988. Graphical display of estimates having differing standard errors. *Technometrics*, 30: 271–281.

Galbraith, R. F., 1990. The Radial Plot: Graphical assessment of spread in ages. *International Journal of Radiation Applications and Instrumentation. Part D. Nuclear Tracks and Radiation Measurements*, 17: 207–214.

Gedl, P., 1997. Palynological study of an olistolith from the so-called Sucha formation, Zawoja IG-1 borehole (Flysch Carpathians, Poland): age and palaeoenvironment. *Annales Societatis Geologorum Poloniae*, 67: 203–215.

Gleadow, A. J. W., 1981. Fission-track dating methods: What are the real alternatives? *Nuclear Tracks*, 5: 3–14.

Gleadow, A. J. W., Duddy, I. R., Green, P. F. & Hegarty, K. A., 1986. Fission track lengths in the apatite annealing zone and the interpretation of mixed ages. *Earth and Planetary Science Letters*, 78: 245–254.

Golonka, J., Gahagan, L., Krobicki, M., Marko, F., Oszczypko, N. & Ślączka, A., 2006. Plate-tectonic evolution and paleogeography of the Circum-Carpathian region. In: Golonka, J. & Picha, F. J. (eds), *The Carpathians and Their Foreland: Geology and Hydrocarbon Resources. AAPG Memoir,* 84: 11–46.

Golonka, J. & Waśkowska, A., 2012. The Beloveža Formation of the Rača Unit in the Beskid Niski Mts. (Magura Nappe, Polish Flysch Carpathians) and adjacent parts of Slovakia and their equivalents in the western part of the Magura Nappe; Remarks on the Beloveža Formation – Hieroglyphic Beds. *Geological Quarterly*, 56: 821–832.

Hurai, V., Marko, F., Tokarski, A. K., Świerczewska, A., Kotulová, J. & Biroň, A., 2006. Fluid inclusion evidence for deep burial of the Tertiary accretionary wedge of the Carpathians. *Terra Nova*, 18: 440–446.

Hurford, A. J., 1990. Standardization of fission track dating calibration: Recommendation by the Fission Track Working Group of the I.U.G.S. Subcommission on Geochronology. *Chemical Geology (Isotope Geoscience Section)*, 80: 171–178.

Hurford, A. J. & Green, P. F., 1982. A users' guide to fission track dating calibration. *Earth and Planetary Science Letters*, 59: 343–354.

Jiříček, R., 1979. Tectonic development of the Carpathian arc in the Oligocene and Neogene. In: Machel, M. (ed.), *Tektonické profily západními Karpaty*. Geologicky Ústav Dionýza Štúra, Bratislava, pp. 203–214.

Jonckheere, R., Ratschbacher, L. & Wagner, G. A., 2003. A repositioning technique for counting induced fission tracks in muscovite external detectors in single-grain dating of minerals with low and inhomogeneous uranium concentrations. *Radiation Measurements*, 37: 217–219.

Kiss, A., Gellért, B. & Fodor, L., 2001. Structural history of the Porva Basin in the Northern Bakony MTS (Western Hungary): Implications for the Mesozoic and tertiary tectonic evolution of the Transdanubian range and Pannonian Basin. *Geologica Carpathica*, 52: 183–190.

Kováč, M., Márton, E., Oszczypko, N., Vojtko, R., Hók, J., Králiková, S., Plašienka, D., Klučiar, T., Hudáčková, N. & Oszczypko-Clowes, M., 2017. Neogene palaeogeography and basin evolution of the Western Carpathians, Northern Pannonian domain and adjoining areas. *Global and Planetary Change*, 155: 133–154.

Kováč, M., Plašienka, D., Soták, J., Vojtko, R., Oszczypko, N., Less, G., Ćosović, V., Fügenschuh, B. & Králiková, S., 2016. Paleogene palaeogeography and basin evolution of the Western Carpathians, Northern Pannonian domain and adjoining areas. *Global and Planetary Change*, 140: 9–27.

Książkiewicz, M., 1958. Sedimentation in the Carpathian Flysch sea. *Geologische Rundschau*, 47: 418–425.

Książkiewicz, M., 1977. The tectonics of the Carpathians. In: Pożaryski, W. (ed.), *Geology of Poland*, *Vol. 4*, *Tectonics.* Wydawnictwa Geologiczne, Warsaw, pp. 476–620.

Lexa, J., Bezák, V., Elečko, M., Mello, J., Polák, M., Potfaj, M., Vozár, J., Schnabel, G. W., Pálenský, P. & Császár, G., 2000. *Geological Map of Western Carpathians and Adjacent Areas 1: 500 000.* Geological Survey of Slovak Republic, Bratislava.

Márton, E., 2020. Last scene in the large-scale rotations of the Western Carpathians as reflected in paleomagnetic constraints. *Geology, Geophysics and Environment*, 46: 109–133.

Matenco, L. & Bertotti, G., 2000. Tertiary tectonic evolution of the external East Carpathians (Romania). *Tectonophysics*, 316: 255–286.

Mazzoli, S., Jankowski, L., Szaniawski, R. & Zattin, M., 2010. Low-T thermochronometric evidence for post-thrusting (< 11 Ma) exhumation in the Western Outer Carpathians, Poland. *Comptes Rendus – Geoscience*, 342: 162–169.

McDowell, F. W., McIntosh, W. C. & Farley, K. A., 2005. A precise ^{40}Ar-^{39}Ar reference age for the Durango apatite (U-Th)/He and fission-track dating standard. *Chemical Geology*, 214: 249–263.

Mikołajczak, M., Barmuta, J., Ponikowska, M., Mazur, S. & Starzec, K., 2021. Depth-to-basement study for the western Polish Outer Carpathians from three-dimensional joint inversion of gravity and magnetic data. *Journal of Geosciences (Czech Republic)*, 66: 15–36.

Min, M., Enkelmann, E., Jonckheere, R., Trautmann, C. & Ratschbacher, L., 2007. Measurements of fossil confined fission tracks in ion-irradiated apatite samples with low track densities. *Nuclear Instruments and Methods in Physics Research, Section B: Beam Interactions with Materials and Atoms*, 259: 943–950.

Morley, C. K., 1996. Models for relative motion of crustal blocks within the Carpathian region, based on restorations of the outer Carpathian thrust sheets. *Tectonics*, 15: 885–904.

Nakapelyukh, M., Bubniak, I., Bubniak, A., Jonckheere, R. & Ratschbacher, L., 2018. Cenozoic structural evolution, thermal history, and erosion of the Ukrainian Carpathians fold-thrust belt. *Tectonophysics*, 722: 197–209.

Nemčok, M., Dilov, T., Wojtaszek, M., Ludhová, L., Klecker, R. A., Sercombe, W. J. & Coward, M. P., 2007. Dynamics of the Polish and Eastern Slovakian parts of the Carpathian accretionary wedge: insights from palaeostress analyses. *Geological Society, London, Special Publications*, 272: 271–302.

Nemčok, M., Hok, J., Kovac, P., Marko, F., Coward, M. P., Madaras, J., Houghton, J. J. & Bezak, V., 1998b. Tertiary extension development and extension/compression interplay in the West Carpathian mountain belt. *Tectonophysics*, 290: 137–167.

Nemčok, M., Kovác, D. & Lisle, R. J., 1999. A stress inversion procedure for polyphase calcite twin and fault/slip data sets. *Journal of Structural Geology*, 21: 597–611.

Nemčok, M., Krzywiec, P., Wojtaszek, M., Ludhová, L., Klecker, R. A., Sercombe, W. J. & Coward, M. P., 2006b. Tertiary development of the Polish and eastern Slovak parts of the Carpathian accretionary wedge: Insights from balanced cross-sections. *Geologica Carpathica*, 57: 355–370.

Nemčok, M., Nemčok, J., Wojtaszek, M., Ludhová, L., Oszczypko, N., Sercombe, W. J., Cieszkowski, M., Paul, Z., Coward, M. P. & Ślączka, A., 2001. Reconstruction of Cretaceous rifts incorporated in the Outer West Carpathian wedge by balancing. *Marine and Petroleum Geology*, 18: 39–64.

Nemčok, M., Pogácsás, G. & Pospíšil, L., 2006a. Activity timing of the main tectonic systems in the Carpathian–Pannonian region in relation to the rollback destruction of the lithosphere. In: Golonka, J. & Picha, F. J. (eds), *The Carpathians and Their Foreland: Geology and Hydrocarbon Resources. AAPG Memoir,* 84: 743–766.

Nemčok, M., Pospisil, L., Lexa, J. & Donelick, R. A., 1998a. Tertiary subduction and slab break-off model of the Carpathian–Pannonian region. *Tectonophysics*, 295: 307–340.

Nescieruk, P. & Wójcik, A., 2001. *Szczegółowa Mapa Geologiczna Polski w skali 1:50 000, arkusz Skoczów (1011)*. Wydawnictwa Geologiczne, Warszawa. [In Polish.]

Oszczypko, N., 1997. The Early–Middle Miocene Carpathian peripheral foreland basin (Western Carpathians, Poland). *Przegląd Geologiczny*, 45: 1054–1063.

Oszczypko, N., Golonka, J., Malata, T., Poprawa, P., Słomka, T. & Uchman, A., 2003. Tectono-stratigraphic evolution of the Outer Carpathian basins (Western Carpathians, Poland). *Mineralia Slovaca*, 35: 17–20.

Oszczypko, N., Malata, E., Bąk, K., Kędzierski, M. & Oszczypko-Clowes, M., 2005. Lithostratigraphy and biostratigraphy of the Upper Albian–Lower/Middle Eocene flysch deposits in the Bystrica and Rača subunits of the Magura Nappe (Beskid Wyspowy and Gorce Ranges, Poland). *Annales Societatis Geologorum Poloniae*, 75: 27–69.

Oszczypko, N. & Oszczypko-Clowes, M., 2009. Stages in the Magura Basin: a case study of the Polish sector (Western Carpathians). *Geodinamica Acta*, 22: 83–100.

Passchier, C. W. & Trouw, R. A. J., 2005. *Microtectonics*. *2nd Edition.* Springer, Berlin, 366 pp.

Paul, Z., Ryłko, W. & Tomaś, A., 1996. Geological structure of the western part of the Polish Carpathians. *Kwartalnik Geologiczny*, 40: 501–520.

Picha, F. J. & Stránik, Z., 1999. Late Cretaceous to early Miocene deposits of the Carpathian foreland basin in southern Moravia. *International Journal of Earth Sciences*, 88: 475–495.

Picha, F. J., Stránik, Z. & Krejči, O., 2006. Geology and hydrocarbon resources of the Outer Western Carpathians and their foreland, Czech Republic. In: Golonka, J. & Picha, F. J. (eds), *The Carpathians and Their Foreland: Geology and Hydrocarbon Resources. AAPG Memoir,* 84: 49–175.

Plašienka, D., Aubrecht, R., Bezák, V., Bielik, M., Broska, I., Bučová, J., Fekete, K. & Gaži, P., 2021. *Structure, Composition and Tectonic Evolution of the Pieniny Klippen Belt – Central Western Carpathians Contiguous Zone (Kysuce and Orava Regions, NW Slovakia)*. Comenius University, Bratislava, 148 pp.

Połtowicz, S., 2004. Miocen parautochtoniczny i olistoplaki fliszowe polskich Karpat Zachodnich. *Geologia*, 30: 389–405. [In Polish.]

Potfaj, M., Maglay, J., Šlepecky, T. & Teťak, F., 2002. *Geological Map of the Kysuce Region 1: 50 000.* Bratislava, ŠGUDŠ.

Ratschbacher, L., Frisch, W., Linzer, H. & Merle, O., 1991a. Lateral extrusion in the Eastern Alps, part 2: structural analysis. *Tectonics*, 10: 257–271.

Ratschbacher, L., Merle, O., Davy, P. & Cobbold, P., 1991b. Lateral extrusion in the Eastern Alps, part 1: boundary conditions and experiments scaled for gravity. *Tectonics*, 10: 245–256.

Roca, E., Bessereau, G., Jawor, E., Kotarba, M. & Roure, F., 1995. Pre-Neogene evolution of the Western Carpathians: Constraints from the Bochnia-Tatra Mountains section (Polish Western Carpathians). *Tectonics*, 14: 855–873.

Roebben, G., Ingelbrecht, C. & Derbyshire, M., 2006. *Certification of Uranium Mass Fraction in IRMM-540R and IRMM-541 Uranium-doped Oxide Glasses*. Publications Office, Institute for Reference Materials and Measurements, Reference Material Unit, Geel, Belgium, 29 pp.

Roger, M., de Leeuw, A., van der Beek, P., Husson, L., Sobel, E. R., Glodny, J. & Bernet, M., 2023. Construction of the Ukrainian Carpathian wedge from low-temperature thermochronology and tectono-stratigraphic analysis. *Solid Earth*, 14: 153–179.

Roure, F., Roca, E. & Sassi, W., 1993. The Neogene evolution of the outer Carpathian flysch units (Poland, Ukraine and Romania): kinematics of a foreland/fold-and-thrust belt system. *Sedimentary Geology*, 86: 177–201.

Roure, F. & Sassi, W., 1995. Kinematics of deformation and petroleum system appraisal in Neogene foreland fold-and-thrust belts. *Petroleum Geoscience*, 1: 253–269.

Rubinkiewicz, J., 2000. Development of fault pattern in the Silesian nappe: Eastern Outer Carpathians, Poland. *Geological Quarterly*, 44: 391–404.

Rubinkiewicz, J., 2007. Fold-thrust-belt geometry and detailed structural evolution of the Silesian nappe – Eastern part of the Polish Outer Carpathians (Bieszczady Mts.). *Acta Geologica Polonica*, 57: 479–508.

Ryłko, W., 2018. *Szczegółowa Mapa Geologiczna Polski w skali 1:50 000, arkusz Milówka*. Wydawnictwa Geologiczne, Warszawa. [In Polish.]

Ryłko, W., Żytko, K. & Rączkowski, W., 1992. *Objaśnienia do Szczegółowej Mapy Geologicznej Polski w skali 1: 50 000, arkusz Czadca-Ujsoły*. Wydawnictwa Geologiczne, Warszawa, 78 pp. [In Polish.]

Ryłko, W., Żytko, K., Rączkowski, W. & Wójcik, A., 1993. *Szczegółowa Mapa Geologiczna Polski w skali 1:50 000,arkusz Czadca-Ujsoły.* Wydawnictwa Geologiczne, Warszawa. [In Polish.]

Schmid, S. M., Fügenschuh, B., Kounov, A., Matenco, L., Nievergelt, P., Oberhänsli, R., Pleuger, J., Schefer, S., Schuster, R. & Tomljenović, B., 2020. Tectonic units of the Alpine collision zone between Eastern Alps and western Turkey. *Gondwana Research*, 78: 308–374.

Ślączka, A., Krugłov, S., Golonka, J., Oszczypko, N. & Popadyuk, I., 2006. Geology and hydrocarbon resources of the Outer Carpathians, Poland, Slovakia, and Ukraine: General Geology. In: Golonka, J. & Picha, F. J. (eds), *The Carpathians and Their Foreland: Geology and Hydrocarbon Resources*. *AAPG Memoir,* 84: 221–258.

Słomka, T. & Słomka, E., 2001. Sequences of the lithofacies and depositional intervals in the Godula Beds of the Polish Outer Carpathians. *Annales Societatis Geologorum Poloniae*, 71: 35–42.

Spang, J. H., 1972. Numerical method for dynamic analysis of calcite twin lamellae. *Geological Society of America Bulletin*, 83: 467–472.

Sperner, B. & Ratschbacher, L., 1994. A Turbo Pascal program package for graphical presentation and stress analysis of calcite deformation. *Zeitschrift der Deutschen Geologischen Gesellschaft*, 145: 414–423.

Sperner, B., Ratschbacher, L. & Nemčok, M., 2002. Interplay between subduction retreat and lateral extrusion: Tectonics of the Western Carpathians. *Tectonics*, 21: 1–24.

Sperner, B., Ratschbacher, L. & Ott, R., 1993. Fault-striae analysis: a Turbo Pascal program package for graphical presentation and reduced stress tensor calculation. *Computers & Geosciences*, 19: 1361–1388.

Sperner, B. & Zweigel, P., 2010. A plea for more caution in fault-slip analysis. *Tectonophysics*, 482: 29–41.

Starzec, K., Schnabel, W., Szotek, A. & Pastucha, M., 2014. *Updating of the Surface Geological Map in Frame of the Project "Seismic Data Acquisition Sól 2D*. Unpublished Map, Geokrak Company, Kraków.

Stráník, Z., 1963. Tectonic structure of the southern part of the Zdanice unit. *Geologické Práce, Správy*, 28: 155–160.

Strzeboński, P., 2015. Late Cretaceous–early Paleogene sandy-to-gravelly debris flows and their sediments in the Silesian Basin of the Alpine Tethys (Western Outer Carpathians, Istebna Formation). *Geological Quarterly*, 59: 195–214.

Strzeboński, P., 2022. Contrasting styles of siliciclastic flysch sedimentation in the Upper Cretaceous of the Silesian Unit, Outer Western Carpathians: Sedimentology and genetic implications. *Annales Societatis Geologorum Poloniae*, 92: 159–180.

Świerczewska, A., 2005. The interplay of the thermal and structural histories of the Magura Nappe (Outer Carpathians) in Poland and Slovakia. *Mineralogia Polonica*, 36: 91–144.

Świerczewska, A. & Tokarski, A. K., 1998. Deformation bands and the history of folding in the Magura nappe, Western Outer Carpathians (Poland). *Tectonophysics*, 297: 73–90.

Teťák, F., Cieszkowski, M., Golonka, J., Waśkowska, A. & Szczęch, M., 2017. The Ropianka Formation of the Bystrica Zone (Magura Nappe, Outer Carpathians): proposal for a new reference section in northwestern Orava. *Annales Societatis Geologorum Poloniae*, 87: 259–274.

Vermeesch, P., 2009. RadialPlotter: A Java application for fission track, luminescence and other radial plots. *Radiation Measurements*, 44: 409–410.

Wójcik, A. & Jugowiec, M., 1998. The youngest members of the folded Miocene in the Andrychów region (Southern Poland). *Przegląd Geologiczny*, 46: 763–770.

Wójcik, A., Marciniec, P. & Nescieruk, P., 2001. Tectonic units in the zone of the Carpathian overthrust – the folded Miocene between Zebrzydowice and Andrychów (the Andrychów Unit). *Biuletyn Państwowego Instytutu Geologicznego*, 396: 164–166.

Wójcik, A. & Nescieruk, P., 2000. *Szczegółowa Mapa Geologiczna Polski w skali 1:50 000, arkusz Pszczyna.* Wydawnictwa Geologiczne, Warszawa. [In Polish.]

Zattin, M., Andreucci, B., Jankowski, L., Mazzoli, S. & Szaniawski, R., 2011. Neogene exhumation in the Outer Western Carpathians. *Terra Nova*, 23: 283–291.

Zuchiewicz, W., Tokarski, A. K., Jarosiński, M. & Márton, E., 2001. Late Miocene to present day structural development of the Polish segment of the Outer Carpathians. *Stephan Mueller Special Publication Series*, 3: 185–202.

Żytko, K., 1963. *Szczegółowa Mapa Geologiczna Polski w skali 1:50 000, arkusz Milówka*. Wydawnictwa Geologiczne, Warszawa. [In Polish.]